Transition from a Townsend discharge to a normal discharge via two-dimensional modeling

V. I. Kolobov* and A. Fiala

Centre de Physique Atomique de Toulouse, Université Paul Sabatier, 118 route de Narbonne, 31062 Toulouse Cedex, France
(Received 22 December 1993; revised manuscript received 15 April 1994)

The transition from a Townsend discharge to a normal discharge is investigated using a two-dimensional numerical model and an approximate analysis. The numerical model is based on a fluid description of electron and ion transport coupled with Poisson's equation, with the ionization source depending on the local field strength or provided by a Monte Carlo simulation of the fast electrons. The model is applied to an argon discharge, for a product of pressure and gap length in the 1–10 Torr cm range. The proposed analytical model provides insight into the major physical phenomena observed experimentally in the subnormal glow region: the lateral constriction of the Townsend discharge with an increase of the current, the negative differential resistance of the discharge with a hysteresis loop in the current-voltage characteristics, and the appearance of current oscillations and their dependence on parameters of the external circuit. The field distortion is responsible for the constriction of the Townsend discharge provided that either the sign of the second derivative of the ionization coefficient α with respect to the electric field strength E is positive or the secondary emission coefficient γ is an increasing function of E. A simple analytical description of nonlocal ionization is also suggested. Subnormal oscillations are treated as a two-dimensional phenomenon.

PACS number(s): 52.80.Hc, 51.50.+v, 52.40.Hf

I. INTRODUCTION

Interest in glow discharges has been growing recently because of numerous applications (plasma processing) and rapid progress in numerical modeling. A number of old problems in gas discharge physics have been solved in recent years, and others are still under investigation. One such classical problem is the existence of different regimes of glow discharges (subnormal, normal, and abnormal) between parallel plane electrodes [1,2]. It was experimentally observed that in a subnormal glow regime, between the Townsend discharge and the normal glow discharge, rather complex two-dimensional nonstationary discharge modes exist. Recently this regime has been studied experimentally and theoretically in a number of publications [3–8], but some of the physical properties of this regime still need to be clarified. The goal of this paper is to study the transition between a Townsend discharge and a normal discharge by means of numerical modeling and to develop a simplified description of these phenomena.

We present here results from two-dimensional numerical modeling of the subnormal glow regime based on the method described in Ref. [9]. The set of fluid equations coupled to Poisson's equation is solved with the ionization source either given in a local approximation by the Townsend coefficient $\alpha(E)$ or provided by a Monte Carlo simulation of the fast electrons. The simulations are done for argon in a cylindrical $R = 1.5$ cm radius chamber,

with the product of pressure and gap length pL in the range 1–10 Torr cm. The secondary emission coefficient γ was set to 0.07 in the numerical calculations.

The suggested analytical approach provides insight into the main physical phenomena in the subnormal regime. The distortion of the field is shown to be responsible for the constriction of the Townsend discharge provided that the second derivative of $\alpha(E)$ with respect to the electric field strength is positive. The role of a possible dependence of secondary emission coefficient $\gamma(E)$ on the electric field strength is also analyzed and is shown to be important in the region where the current vanishes. Both these factors may cause the instability of Townsend discharge. The analytical model predicts the negative slope of the current-voltage characteristics in the region of instability and show that current oscillations can appear and are accompanied by a considerable variation in the radial shape of the discharge.

The structure of the paper is as follows. In Sec. II, the major physical phenomena observed in the subnormal glow region are sketched and a review of previous work is given. Section III is devoted to numerical modeling. The analytical approach is formulated in Sec. IV. The results of the calculations are discussed in Sec. V and summarized in Sec. VI. A simple model for nonlocal ionization is suggested and the electron multiplication coefficient is calculated in the Appendix.

II. TOWNSEND BREAKDOWN AND GLOW DISCHARGE MODES

The breakdown of a plane-parallel discharge gap is characterized by a Paschen curve which depicts the dependence of the breakdown voltage U_t on the product of gas pressure p and gap length L [10]. For given gas and cathode material, the Paschen curve exhibits a

---
*Author to whom correspondence should be addressed. Present address: Engineering Research Center for Plasma-Aided Manufacturing, University of Wisconsin-Madison, 1410 Johnson Drive, Room 101, Madison, WI 53706-1608.

minimum at $(pL) = (pL)_{min}$, corresponding to optimal conditions for the development of the electron avalanche. The breakdown voltage ensures the primitive reproduction of electrons in the gap. If a single electron emitted by the cathode produces $M - 1$ positive ions (M being the electron multiplication), which, hitting the cathode, liberate γ electrons per ion, then one primary electron is replaced with one secondary electron: the electron reproduction coefficient $\eta = \gamma(M - 1)$ is equal to unity $\eta = 1$. The onset of breakdown needs at least a small overvoltage $\Delta U = U - U_t$, ensuring expanded reproduction of electrons $\eta > 1$. The current increases during breakdown (when $U > U_t$) with the time scale $\eta \tau_i / (\eta - 1)$, where τ_i denotes the ion transit time from the anode to the cathode. When the current J increases, an increasing voltage JR_c is dropped across the Ohmic resistance of the circuit R_c and the voltage across the electrodes decreases. When U drops to U_t, the current ceases to grow and the self-sustaining current becomes stationary. Which discharge mode will be set up depends on the supplied voltage and the value of R_c.

The relation between current density j, pressure p, maintaining voltage U, and gap length L is shown in Fig. 1 for a steady-state self-sustained discharge between two plane-parallel electrodes of radius R much larger than L [1]. There is no completely agreed upon nomenclature for discharge forms. A Townsend discharge will be taken to be one lacking appreciable space charge and characterized by a maintaining voltage which is independent of the current. The discharge voltage is therefore equal to the breakdown potential and the U versus pL curve in Fig. 1 represents a Paschen curve having a minimum at $(pL)_{min}$. The plateau 3 with the lowest maintaining voltage is the region of normal discharges. The plateau gradually narrows with reduction of pL and at $pL < (pL)_{min}$ transforms
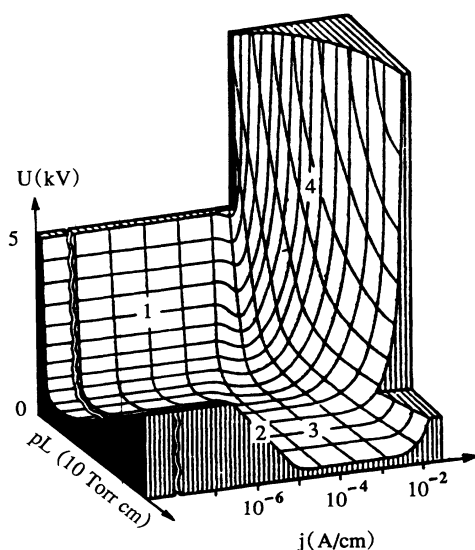

FIG. 1. Diagrammatic representation of different types of glow discharges between plane-parallel electrodes (from Klyarfeld, Guseva, and Pokrovskaya-Soboleva [1]). 1, Townsend discharge; 2, subnormal discharge; 3, normal discharge; 4, abnormal discharge.

into an initially deep, then gradually disappearing, depression which separates the regions of subnormal and abnormal discharges. The subnormal region 2 occupying the transition region between the Townsend and normal discharges and characterized by a descending part of the current-voltage characteristic is omitted from Klyarfeld, Guseva, and Pokrovskaya-Soboleva's classification [1].

The Townsend discharge covers the whole area of the cathode. The subnormal discharge at $pL > (pL)_{min}$ constricts radially as the current is increased [2]. A considerable constriction of the radial distributions of the current density and light emission over the area of the cathode has been observed for very low currents [4]. After the switch to the normal discharge, which at first has about the same transverse dimensions as its subnormal precursor, the discharge reexpands radially with a further increase in the current. The current increases due to changes of the area through which the current flows while the current density remains unchanged. For $pL < (pL)_{min}$ there is a direct transition from a subnormal to an abnormal discharge. The transition occurs without radial constriction; the subnormal and abnormal discharges cover the whole area of the cathode apart from any wall sheaths.

Different types of transition to the normal regime have been observed experimentally depending on gas, the value of pL, and parameters of the external circuit [5]. It has been found that for values of the time constant $\tau = R_c C$ (the product of the resistance and the capacitance of the circuit) less than a limiting value τ_{lim}, a static transition can be obtained [5]. Small amplitude oscillations of current observed at $\tau \gtrsim \tau_{lim}$ do not fundamentally alter the transverse shape of the discharge and cease with further current rise before an essentially lateral constriction occurs. A static discharge that arises after the oscillations cease goes over to a normal discharge with a further increase of the current. The increase of τ leads to the extension of the region of instability and to the appearance of relaxation oscillations accompanied by lateral constriction of the discharge in the oscillation region. Relaxation oscillations of large amplitude cease only when a normal cathode spot is formed [4]. On the left of the Paschen's minimum, the value of τ_{lim} increases sharply with a reduction of pL. On the right branch, the region of stability of the Townsend discharge shifts toward lower currents with increasing pL. The reverse transition from the normal discharge to the Townsend one is accompanied by a hysteresis loop [3,4,7,8].

No systematic experimental investigation of the radial shape of the discharge in the subnormal glow regime has been published. Strong constriction of the light emission has been reported [2] for subnormal discharges in air for large enough pL values of about 25 Torr cm. The lateral constriction of the current density and light emission has been recorded [6] for discharges operating near Paschen's minimum. A sharp constriction of the light emission has been observed for neon discharges on the right branch of the Paschen curve for pressure in the 50–200 Torr range and gap length between 0.1 and 0.7 cm [7]. Subnormal oscillations have been investigated in a number of works (see the references cited in [6]) including a detailed study

of the dependence of their properties on parameters of the external circuit [5]. A theory of oscillations has been proposed [4,6], based on small perturbations of the field and neglecting the alterations in the radial shape of the discharge. As a two-dimensional phenomenon they were treated by Hollo and Nyiri [11].

III. NUMERICAL MODELING

In the modern modeling of low-pressure, direct current glow discharges, a fluid approximation for the slow electrons is often used as well as some type of kinetic simulation of the fast electrons, which are far from equilibrium with the electric field. The most advanced one-dimensional models of direct current discharges have been published in Refs. [12–14]. Two-dimensional numerical models have also been developed [8,9,15,16]. Steady-state subnormal discharges have been calculated by Schweigert [8] using a two-dimensional fluid model with the local approximation for the ionization rate and by Fiala, Pitchford, and Boeuf [9] with the ionization source provided by a Monte Carlo simulation of the fast electrons.

A. Basic equations

For numerical discharge modeling in the considered range of parameters (Fig. 1), the set of fluid equations for charged particle transport coupled with Poisson's equation for the electric field can be used [8,9]

$$\frac{\partial n_i}{\partial t} + \mathrm{div}\, n_i \mu_i \mathbf{E} = I \ , \tag{1}$$

$$\frac{\partial n_e}{\partial t} + \mathrm{div}(n_e \mu_e \mathbf{E}) - D_e \Delta n_e = I \ , \tag{2}$$

$$\Delta \phi = 4\pi e(n_e - n_i), \quad \mathbf{E} = -\nabla \phi \ , \tag{3}$$

with boundary conditions

$$n_e(z=0) = \gamma \frac{\mu_i}{\mu_e} n_i(z=0), \quad n_i(z=L) = n_e(z=L) = 0 \ ,$$

$$n_e(r=R)=0, \quad \frac{\partial \phi}{\partial r}(r=R) = -4\pi\sigma \ , \tag{4}$$

$$\phi(z=0)=0, \quad \phi(z=L)=U \ ,$$

where n_e and n_i are the electron and ion densities, μ_i and μ_e their mobilities, D_e is the electron diffusion coefficient, γ the secondary emission coefficient, L the gap length, R the radius of the discharge tube, U the maintaining voltage, I the ionization rate, and σ the surface charge density of the dielectric wall. Use of Eqs. (1)–(4) implies that the physical processes under study are characterized by

the time scale corresponding to the ion transit time and ionization frequency [10]. The calculations were done using both the local approximation for the ionization rate $I = v_e \alpha n_e$, where $\alpha(E)$ is the Townsend coefficient, and the ionization rate I provided by a Monte Carlo simulation of the fast electrons. The electron mobility and diffusion coefficient are assumed to be field independent and their ratio D_e/μ_e corresponds to the temperature of slow electrons $T_e = D_e/\mu_e = 1$ eV. The diffusion of ions is neglected provided that the electron temperature exceeds greatly the ion temperature. The electron current to the cathode is mobility dominated, but to the anode and to the walls it is purely due to electron diffusion. Ion flux from the anode is absent. The electron emission flux from the cathode is proportional to the ion flux.

Gas heating is neglected. Argon is used as a working gas. The transport coefficients and data used in the Monte Carlo simulation of the fast electrons as well as the detailed description of the numerical method can be found in Ref. [9]. The applicability of the fluid model for the description of electron transport is discussed in Sec. V.

The gap voltage U is calculated according to

$$U = U_s - R_c J \ , \tag{5}$$

where U_s is the voltage of the generator, R_C the resistance of the external circuit, and J the discharge current. The steady-state solutions of (1)–(4) were found by following the time evolution of the discharge. The current-voltage characteristics of the transition region between the Townsend and normal discharges were obtained by changing the value of the resistance in (5).

B. Numerical results

Numerical modeling of the subnormal region of dc glow discharges operating on the right branch of the Paschen curve allows us to reproduce the major physical phenomena observed in this region: (i) constriction of the Townsend discharge with an increase in current, (ii) the negative slope of the current-voltage characteristics in the transition region, and (iii) formation of the normal cathode spot and increase of its size with further current rise. Using the Monte Carlo simulation of the fast electrons to reflect the nonlocal nature of the ionization in the cathode region results in formation of a plasma density maximum and the occurrence of the axial field reversals in the plasma region of the normal discharge. Oscillations do not appear in the numerical modeling because

TABLE I. Discharge parameters obtained from numerical modeling for pressure $p = 10$ Torr: current J, maintaining voltage U, resistance of the external circuit R_c, electric field on the cathode and on the anode E_c and E_a, and maximal values of ion and electron densities n_p and n_e.

10 Torr	J (μA)	U (V)	R_c (kΩ)	E_c (V/cm)	E_a (V/cm)	n_p (10^8 cm^{-3})	n_e (10^8 cm^{-3})
a	0.07	325.6	1000	329	324	4.8×10^{-2}	1.5×10^{-4}
b	1.50	324.8	50	400	277	1.23	6.3×10^{-3}
c	1.69	323.8	45	449	245	2.61	2.2×10^{-2}
d	2.31	319.2	35	554	175	7.3	0.24
e	2.87	314.0	30	630	139	11.8	0.96

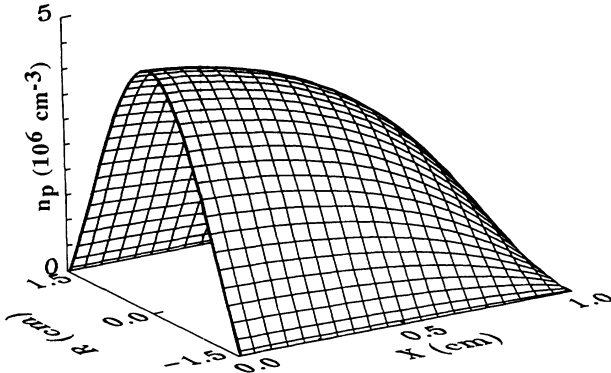FIG. 2. Two-dimensional spatial distribution of the ion density in a Townsend discharge for the conditions shown in Table I, line *b*.

FIG. 4. (a) Equipotential lines, (b) contours of constant ionization, (c) electrons, and (d) ion density for a constricted subnormal discharge at 10 Torr (Table I, line *d*). Ten equidistant levels between the maximum and the level 0.1 are shown. A local approximation for the ionization is used.

the displacement current and capacitance of the external circuit are not included in Eq. (5). The appearance of oscillations is analyzed in Sec. IV B 3 using the analytical model.

In this section we present some typical results from numerical modeling. The simulations were performed for the pL range 3–10 Torr cm, which corresponds to the right branch of the Paschen curve $(pL)_{min} \sim 1$ Torr cm [10].

Figure 2 shows the distribution of the ion density in the Townsend discharge at $p = 10$ Torr. In the Townsend discharge, practically the entire space between the electrodes is positively charged, but for low currents the space charge is small and the external electric field is only slightly distorted (see Table I). The calculated radial profile of the ion density is well reproduced by a Bessel function (dashed line in Fig. 2). The maximum of the ion density is reached at the cathode. The maxima of the electron density and ionization are located in the vicinity of the anode and are shifted toward the cathode with reduction of pressure. The field decreases in the vicinity of the anode and increases in the vicinity of the cathode, more the higher the current (Table I). The distortion of the electric field results in lateral constriction of the discharge (Fig. 3). Finally, the maximum of the ion density forms in the center of the gap due to the curvature of
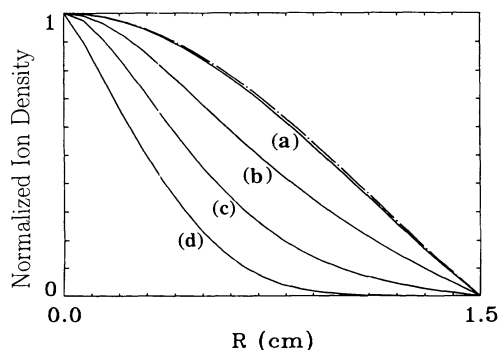

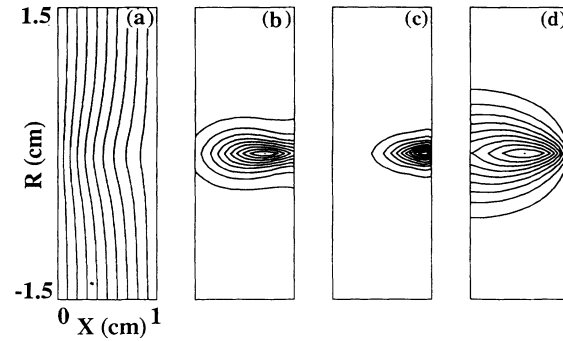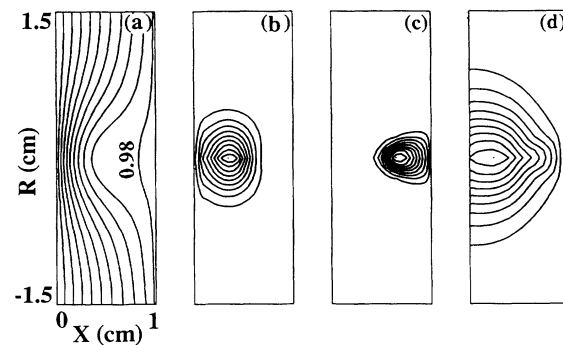FIG. 5. (a) Equipotential lines, (b) contours of constant ionization, (c) electrons, and (d) ion density for a constricted subnormal discharge at 3 Torr. The ionization is provided by the Monte Carlo simulation of the fast electrons. $U = 144$ V and $J = 14 \mu A$. The maximal values of ionization, electron, and ion density are 5×10^{14} cm^{-3}s^{-1}, 4×10^{8} cm^{-3}, and 10^{9} cm^{-3}, respectively.

FIG. 3. Normalized ion density profiles on the cathode for different currents (see Table I). The dashed line shows the Bessel distribution.
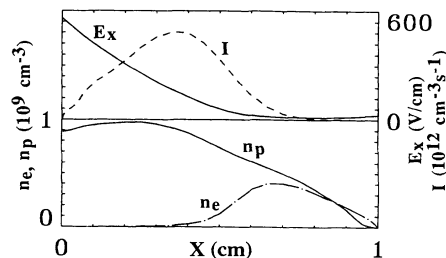

FIG. 6. Axial distributions of the electric field, ionization rate I, and ion and electron densities on the axis of a subnormal discharge for the conditions of Fig. 5.
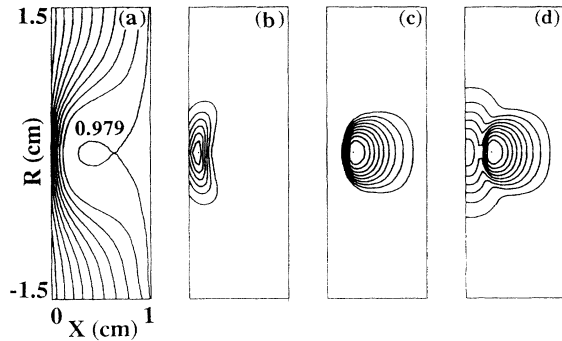
FIG. 7. (a) Equipotential lines, (b) contours of constant ionization, (c) electrons, and (d) ion density for a normal discharge at 3 Torr. The ionization is provided by the Monte Carlo simulation of the fast electrons. $U = 130$ V and $J = 64$ μA. The maximal values of ionization and the plasma density are 4×10^{15} cm^{-3}s^{-1} and 7×10^9 cm^{-3}, respectively. The depth of the potential well is of the order 0.1 V.

the field lines and the maximum of the ionization rate is shifted toward the cathode (Fig. 4). With further increase of the current the cathode sheath and plasma region are formed.

Figures 5–7 show the structure of subnormal and normal discharges at $p = 3$ Torr with an ionization source term provided by a Monte Carlo simulation of the fast electrons. In Fig. 5 the two-dimensional distributions of the potential, the charged particle densities, and the ionization rate are plotted for conditions where the cathode sheath and plasma region are just separated. It is seen that, as above, for 10 Torr, the discharge is already substantially constricted in the lateral direction at these currents. Figure 6 shows the corresponding axial distributions. The length of the cathode sheath can be identified as a position where the electron density is half the ion density. The axial field does not change its sign and reaches its minimum at the point marked by a dot in Fig. 5. The maximum of the ionization is located approximately in the middle of the sheath. The length of the negative glow is about equal to the sheath length.

With further increase of the current, field reversals occur in the plasma and a potential well appears, which captures the slowest electrons. Figure 7 presents the two-dimensional structure of the normal discharge for a spot with a small radius. The depth of the potential well is about 0.1 eV. Small nonlocality of the ionization (the negative glow length slightly exceeds the sheath length) is sufficient for the plasma density maximum to form near the maximum of the potential. The structure of the plasma region is discussed in more detail in Sec. V.

It appears from the numerical simulation that the basic discharge characteristics in the subnormal glow region can be correctly reproduced using a fluid model with a local approach for ionization. For regimes close to normal, the nonlocality of the ionization results in the formation of the plasma density maximum and the appearance of the axial field reversals in the plasma region. This maximum is not so pronounced as in abnormal discharges [9] and thus in the subnormal glow region the ion flux into the sheath (which is proportional to the gradient of the

plasma density on the sheath boundary) is small compared to the total ion flux in the sheath. The results of the numerical modeling help to justify the assumptions made below in the formulation of the simplified model of the discharge.

IV. ANALYTICAL APPROACH

Our analytical approach consists of some approximations which allow us to simplify the initial problem (1)–(4). As the system considered has very different space and time scales, an asymptotic description of the structure formation on the slow space and time scales can be formulated [17]. The time derivative in the electron equation can be neglected and the number of spatial variables can be reduced if the characteristic dimension R of the cross section of the discharge vessel is much greater than the gap length L or the cathode sheath length d. The suggested analytical models describing the formation of the cathode spot can be divided into two groups. The models [8,18,19] account for the radial diffusion of electrons, but neglect the radial component of the field. This assumption restricts the range of applicability of these models to the low-current subnormal regime. It was shown [15,16] that the shape of the normal cathode spot is determined by the two-dimensional distribution of the potential while the electron diffusion does not play a decisive role. The model of the spot including the transport of ions in the radial field has been considered by Hollo and Nyiri [11] with neglect of the radial diffusion of electrons. The approach described below is an extension of the models by Schweigert [8] and Hollo and Nyiri [11].

Two different cases are treated separately in Secs. IV A and IV B. For low currents, the field distortion by the space charge can be considered as a small perturbation. The radial shape of the subnormal discharge is governed in this case by diffusion of electrons and by the form of $\alpha(E)$ and $\gamma(E)$. For larger currents, where the cathode sheath is formed, the radial structure of the discharge is determined by the ion transport in the radial electric field. An equation for the evolution of the cathode sheath in this case is obtained in Sec. IV B and is used for analysis of steady-state and oscillation regimes.

A. Low-current subnormal discharge

In Sec. IV A 1 we ignore the field distortion to obtain an exact solution of the set of fluid equations (1) and (2) for a steady-state case. In Sec. IV A 2 we consider the distortion of the field as a small perturbation and derive an equation governing the time evolution of the radial distribution of the ion space charge. The steady-state solutions of this equation are analyzed in Sec. IV A 3 and the traveling wave solutions are investigated in Sec. IV A 4.

The distortion of the field can be considered as a small perturbation while the ion space charge is small and the gap length greatly exceeds the Poisson length $d = E_0/4\pi en_i$. For this case, using the local approximation for the ionization rate, Eqs. (1) and (2) can be rewritten in the form

$$\frac{\partial n_e}{\partial z} - \lambda_T \frac{1}{r}\frac{\partial}{\partial r} r \frac{\partial n_e}{\partial r} = \alpha n_e , \tag{6}$$

$$\frac{\partial n_i}{\partial t} - v_i \frac{\partial n_i}{\partial z} = v_e \alpha n_e \ , \qquad (7)$$

where v_e and v_i are the electron and ion drift velocities and $\lambda_T = T_e / eE_0$ is the diffusion length. The time derivative in (1) can be omitted provided that $v_e \gg v_i$. At $\lambda_T \alpha \ll 1$, the axial diffusion of electrons can be neglected for the main part of the gap excluding the region of length $\lambda_T \ll 1$ in the vicinity of the anode.

1. Townsend discharge

If $\alpha = \text{const} = \alpha_0$, the linear set of Eqs. (6) and (7) can easily be solved by the method of separation of variables. The steady-state solution has the form

$$n_{e,i}(z,r) = Y_{e,i}(z) J_0(kr) \ , \qquad (8)$$

where $J_0(x)$ is the zeroth-order Bessel function, $k = 2.4/R$, and $Y_{e,i}(z)$ are given by

$$Y_i(z) = Y_i(0) \frac{\exp(\tilde{\alpha}_0 L) - \exp(\tilde{\alpha}_0 z)}{\exp(\tilde{\alpha}_0 L) - 1} \ , \qquad (9)$$

$$Y_e(z) = Y_e(0) \exp(\tilde{\alpha}_0 z) \ , \qquad (10)$$

with

$$\tilde{\alpha}_0 = \alpha_0 - \lambda_T k^2 \ . \qquad (11)$$

As a result of the neglect of axial electron diffusion, the electron density (10) does not satisfy the boundary condition (4) on the anode. The axial diffusion of electrons leads to a density drop near the anode in a length of about $\lambda_T \ll L$. In this region, the electron flux is transformed from the mobility dominated in the bulk to the purely diffusive at the anode. This process should be treated kinetically as discussed in Sec. V.

Using $Y_i(0) = \gamma Y_e(0)$ and $Y_i(L) = 0$, the condition of self-sustenance follows from Eqs. (9) and (10)

$$\frac{1}{\gamma} = \frac{\alpha_0}{\tilde{\alpha}_0} [\exp(\tilde{\alpha}_0 L) - 1] \ . \qquad (12)$$

At $\lambda_T k^2 L \ll 1$, relation (12) coincides with the one-dimensional condition $\gamma[\exp(\alpha_0 L) - 1] = 1$ discussed in Sec. I. The effect of the finite radius R results in the overvoltage $\Delta U = U - U_t = (d\alpha/dE)\lambda_T k^2/\alpha_0$ (U_t is the breakdown voltage at $R \to \infty$, i.e., at $k \to 0$), which is necessary to compensate the losses of electrons to the wall. Consequently, the electron reproduction coefficient $\eta = \gamma[\exp(\alpha_0 L) - 1]$ for a discharge of finite radius R must exceed unity by $\eta - 1 = (\lambda_T k^2/\alpha_0)(\alpha_0 L - 1)$.

The results of the numerical solution of (1)–(4) for low currents [shown in Fig. 2 and in curve (a) of Fig. 3] are well reproduced by Eqs. (8)–(10). This suggests that the radial profile of the ion density for these conditions is governed by the diffusion of electrons. The axial profiles of electron and ion density resemble one-dimensional distributions, i.e., the maximum of the ion density is reached near the cathode and the maxima of the electron density and ionization occur near the anode. In most of the gap the ion density greatly exceeds the electron density, so practically the entire space is positively charged, but the space charge is too small to produce any significant distortion of the external field. The distortion of the field can be evaluated supposing the distribution of the ion density is independent on z, $n_i = n_0 J_0(kr)$. The solution

of Poisson's equation (3) with such a distribution of the space charge is

$$\varphi = \frac{U}{L} \left\{ z + \frac{4\pi e n_0 L}{\kappa^2 U} [A \cosh(kz) + B \sinh(kz) - 1] \right.$$
$$\left. \times J_0(kr) \right\} \ , \qquad (13)$$

where the constants A and B are determined by the conditions $\varphi(z=0) = 0$ and $\varphi(z=L) = U$. For $L \ll R$, the potential profile (13) corresponds to a linear decrease of the axial field $E_z(z,r)$ away from the cathode. If $E_c = E_z(0,r)$ is the field at the cathode, then the point $d = E_c/4\pi e n_0$, where the extrapolated quantity $E_z(z,r)$ vanishes, lies far beyond the discharge gap at low current. As the current increases, it moves closer to the anode and coincides with the anode surface at $n_0 = U/2\pi eL^2$. With a further increase of n_0, at $d < L$, the plasma region is formed.

2. Quasi-one-dimensional model

In this section, we obtain a differential equation describing the evolution of the ion density at the cathode $n_0(r,t)$ for a low-current subnormal discharge at $d \gg L$. Since the distortion of the external field is small, it needs only to be taken into account in $\alpha(E)$. The possible dependence of $\gamma(E)$ will also be considered below. This dependence of $\gamma(E)$ may be responsible for the negative slope of the current-voltage characteristic in this region [4,6].

The space and time scales in the axial and lateral directions differ if $\lambda_T L/R^2 \ll 1$. When the time scale exceeds the ion transit time $\tau_i = L/v_i$, the axial distributions of electron and ion densities at a given radial position can be considered as quasistationary. The radial shape of the discharge is formed on the slow time scale $R^2/\lambda_T v_i \gg \tau_i$.

Using (6) to eliminate the right-hand side in (7) and integrating along the gap, we obtain

$$\frac{\partial}{\partial t} \int_0^L n_i dz + D_e \frac{1}{r} \frac{\partial}{\partial r} r \frac{\partial}{\partial r} \int_0^L n_e(r,z) dz$$
$$= v_e [n_e(L) - n_e(0)] - v_i n_i(0) \ . \qquad (14)$$

To calculate the electron density at the anode we obtain we approximate solution of (6). Equation (6) describes the diffusive spread of the electron avalanche on its way to the anode. At $R^2 \gg \lambda_T L$, this spread is small and the electron density at the anode is given by

$$n_e(L) \approx \left[n_e(0) - \frac{\lambda_T L}{r} \frac{\partial}{\partial r} r \frac{\partial n_e(0)}{\partial r} \right] \exp \int_0^L \alpha(E_z) dz' \ . \qquad (15)$$

Using (10) and (15), we obtain the equation for the ion density on the cathode $n_0(r,t)$ in the form [8]

$$\tau_i \frac{\partial n_0}{\partial t} - \frac{\lambda_T}{\alpha_0} (\alpha_0 L - 1) \frac{1}{r} \frac{\partial}{\partial r} r \frac{\partial n_0}{\partial r} = n_0(\eta - 1) \ , \qquad (16)$$

where

$$\eta(U, n_0) = \gamma \left[\exp \int_0^L \alpha(E_z) dz - 1 \right] \qquad (17)$$

is the electron reproduction coefficient.

To calculate the electron reproduction coefficient (17) we consider small perturbations of the field [4]. The voltage U changes under the influence of the small space charge from U_0 to $U_0 + \Delta U$ and the axial field changes from E_0 to $E_0 + \Delta$, where $\Delta = \Delta U / L + 2\pi e n_0 L (1 - 2z/L)$. For small perturbations, $\alpha(E) \approx \alpha_0 + \alpha'(E - E_0) + \alpha''[(E - E_0)^2 / 2]$, where $\alpha_0 = \alpha(E_0)$, $\gamma(E) \approx \gamma(E_0) + \gamma'(E - E_0)$, and primes denote differentiation with respect to E. The unperturbed value of the electric field E_0 is given by (12). Calculating the integral in (17), we obtain

$$\int_0^L \alpha(E_z) dz \approx \alpha_0 L + \alpha' L \Delta U + \left[\frac{U_0}{L} \right]^2 \frac{\alpha'' N^2 L}{6} , \qquad (18)$$

where $N = 2\pi e n_0 L^2 / U_0$. Using (18), we rewrite (16) in the form

$$\frac{\partial N}{\partial t} - D_1 \frac{1}{r} \frac{\partial}{\partial r} r \frac{\partial N}{\partial r} = \frac{\alpha' U_0 N}{\tau_i} (u + gN + bN^2) , \qquad (19)$$

where $D_1 = \mu_i T_e (1 - 1/L\alpha_0)$, $g = \gamma'/\gamma L \alpha'$, $b = (\alpha''/6\alpha')(U_0/L)$, and $u = \Delta U / U_0$. Equation (19) is a time-dependent diffusion equation with a nonlinear source term known as Fisher's equation in [20]. In our case, the source term also depends parametrically on the discharge maintaining voltage. If the latter is changed with time, a new phenomena compared to [20] appear, as will be discussed below.

It is interesting to note that the diffusion coefficient obtained in (19) coincides in practice with the ambipolar diffusion coefficient $D_a = \mu_i T_e$ though the plasma in the gap is absent. This seemingly unexpected result has a simple explanation [7]. According to (6), the electron avalanche spreads during its motion along the gap by a distance $\sim \sqrt{\lambda_T L}$. The avalanche process is repeated after the time $\tau_i = L / v_i$, which is necessary for the ions (generated mainly in the vicinity of the anode) to reach the cathode surface. Hence during a time t, an initial nonuniformity at the cathode will spread by a length $\sim \sqrt{v_i \lambda_T t}$. The effective diffusion coefficient is therefore of the order of the ambipolar one.

Adopting the usual approximation $\alpha(E) = Ap \exp(-Bp/E)$, we find $b = \frac{1}{3}(BpL/2U - 1)$. The minimum of the Paschen curve corresponds to $BpL/U = 1$ and the point of inflection of $\alpha(E)$ lies to the right of the minimum at $BpL/U = 2$. It follows from Eq. (18) that for $BpL/U > 2$ the conditions for multiplication are facilitated by redistribution of the potential and the same multiplication can be achieved with a lower voltage. If $BpL/U < 2$, the situation is reversed: redistribution either impedes multiplication or increases the voltage. The evolution of the radial shape of the discharge with an increase of the space charge is expected to differ in these two cases.

3. Steady-state analysis

Looking for the steady-state solution of (19), we obtain

$$D_1 N'' + \frac{D_1}{r} N' = -F(N) , \qquad (20)$$

where primes denote differentiation with respect to r and

$F(N) = (\alpha' U_0 N / \tau_i)(u + gN + bN^2)$. Formally, Eq. (20) describes a classical particle of mass D_1 moving in the potential

$$V(N) = \int_0^N F(N') dN' = \frac{\alpha' U_0 N}{2\tau_i} \left[u + \frac{2gN}{3} + \frac{bN^2}{2} \right] \qquad (21)$$

under the influence of a "time"-dependent damping force $-(D_1/r)N'$. The density N plays the role of the particle coordinate and the variable r corresponds to time. The damping force $(D_1/r)N'$ is due to the effect of the cylindrical geometry. It would be absent in a planar case. With the help of this analogy, the formation of the radial structure of the discharge can be analyzed quantitatively. The boundary conditions on the discharge axis $(r = 0)$ and on the wall of the discharge vessel $(r = R)$

$$N'(r = 0) = 0, \quad N(r = R) = 0 \qquad (22)$$

correspond to a particle which starts from a point $N = N_c$ at $r = 0$ with zero velocity N' and reaches the point $N = 0$ after some time R. Multiplying Eq. (20) by N' and integrating over r from 0 to R gives the energy balance of the particle

$$V(N_c, u) - \frac{D_1}{2} N'^2(r = R) = \int_0^R \frac{D_1}{r} N'^2 dr . \qquad (23)$$

According to (23), the alteration in the total energy of the particle has to be equal to the work done by the damping force. For a given N_c, this relationship yields a definite value of the voltage u and thus defines the current-voltage characteristic of the discharge.

Let us consider the case $\alpha' < 0$ $(b < 0)$ when the operating point lies on the Paschen curve between the minimum and the point of inflection $\alpha(E)$. Figure 8 shows the force $F(N)$ for the case when γ is an increasing function of the field [4,6] $g > 0$ and the discharge maintaining voltage is less than the breakdown potential $u < 0$. In this case the function $F(N)$ has two nontrivial roots which correspond to radially uniform solutions of (20). The lower root N_1 decreases whereas the higher N_2 increases with rising u. The root N_1 can be shown to be unstable and the root N_2 is stable [20]. We are interested in a solution which corresponds to a constricted discharge with a radius of the cathode spot less than R. In terms of particle motion, this case represents the particle coming to rest at $N = 0$ with zero velocity [the second term on the left-hand side of (23) vanishes]. In a planar case, such a particle would start from the point where potential passes through zero $V(N_0, u) = 0$ and come to rest at the second maximum of the potential at $N = 0$ (see Fig. 8). The two roots of the potential (21) are given by

$$N_{0,3}(u) = -\frac{2g}{3b} \pm \left[\left[\frac{2g}{3b} \right]^2 - \frac{2u}{b} \right]^{1/2} . \qquad (24)$$

The lower root N_0 increases with a reduction of u until the maximum density $N_n = -2g/3b$ is reached at $u_n = 2g^2/9b$ when the roots join $N_0 = N_3$. As soon as N reaches the value N_n, an increase of the current is accompanied by a rise in the spot radius while the density in the
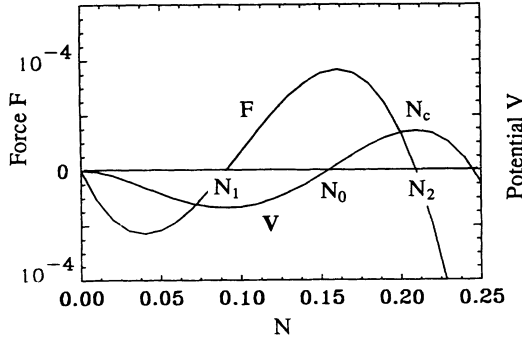
FIG. 8. The force $F(N, \tilde{U})$ acting on the particle and its potential $V(N, \tilde{U})$, in arbitrary units. The particle starts from $N = N_c$, is accelerated in the region $N_c < N < N_1$, and is slowed down in the region $0 < N < N_1$. The discharge parameters correspond to the conditions of curve 5 in Fig. 9.

FIG. 9. Radial distributions of the dimensionless ion density N at $p = 0.5$ Torr for different currents: (1) 4.9 μA, 97.7 V; (2) 7.86 μA, 97.64 V; (3) 10.4 μA, 97.56 V; (4) 19.8 μA, 97.49 V; (5) 39.6 μA, 97.47 V; (6) 79.2 μA, 97.46 V. The secondary emission coefficient γ is an increasing function of the field for $b = -\frac{1}{6}$ and $g = 0.05$.

center remains unchanged $N_c = N_n$. The shape of the large spot is given by

$$N(r) = \frac{N_2}{1 + \exp\left[\left[-\frac{b\hat{a}\alpha}{2\lambda_T}\right]^{1/2} N_2(r - r_0)\right]} , \qquad (25)$$

where $\hat{a} = d \ln\alpha/d \ln E$ and r_0 is the radius of the spot defined as the point where $N(r_0) = N_n/2$.

The term $(1/r)N'$ in Eq. (20) becomes negligible only for a large radius of the spot. For a finite radius, the maintaining voltage u exceeds that of the planar case in order to compensate the work of the damping force. The particle is to start from the point $N_c > N_0$ defined by $V(N_c, u) = \int_0^R (D_1/r)N'^2 dr$ (Fig. 8). For a small radius of the spot, u exceeds u_n and approaches u_n asymptotically with increase of the spot radius when $N_c \sim N_0 \sim N_2$.

The numerical solutions of (20) have been obtained following the time evolution of (19). Figure 9 shows the radial distributions $N(r)$ for different values of u. With an increase of the current, lateral constriction of the discharge occurs while the discharge voltage is slightly reduced. As soon as the density in the center reaches the value corresponding to the maximum of $V(N)$, the lateral spread of the discharge begins. This phenomenon is analogous to the normal-current-density effect discussed below in Sec. IV B 2.

For the case $\alpha'' > 0$ ($b > 0$), the stability of a Townsend discharge is lost for very low currents [7,8]. As the electron multiplication depends strongly on the ion density, the increase of the density in the center cannot be compensated by the lateral diffusion and a sharp constriction of the discharge occurs. Distortion of the field should be taken into account for the description of the constricted discharge, and this is carried out in Sec. IV B.

4. The lateral spread of the discharge

In this section, we will consider time-dependent solutions of Eq. (19) which correspond to traveling waves. Upon application of a constant voltage higher than u_n a lateral spread of the discharge is obtained. Although the model we consider in this section is not applicable to the experimentally investigated case of lateral spread of a
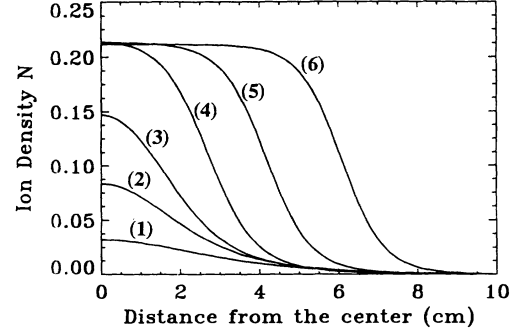
normal discharge [21], the main features of the phenomena are the same and the concept developed here for describing the low-current subnormal discharge will be applicable for the "normal" conditions discussed in Sec. IV B.

In the spatially homogeneous situation, the steady-state solutions of Eq. (19) correspond to the roots of the function $F(N)$. Traveling wave solutions have the form $N(r, t) = N(r - ct) = N(\zeta)$ moving at speed c without change of shape. Equation (19) does not possess traveling wave front solutions in which a wave spreads out with constant speed c, because of the $1/r$ term. But for large r the $(1/r)dN/dr$ term becomes negligible so the solution will tend asymptotically to a traveling wave front solution spreading with constant speed as in the planar case. For this case, substituting the traveling wave form in (19), we obtain an ordinary differential equation

$$D_1 N'' + cN' + AN(N_1 - N)(N - N_2) = 0 , \qquad (26)$$

where $A = -b(\alpha' U_0/\tau_i)$ and primes denote differentiation with respect to ζ. The solution of (26) should satisfy the boundary conditions

$$N(\zeta \to \infty) = 0, \quad N(\zeta \to -\infty) = N_2 . \qquad (27)$$

The set of equations (26) and (27) constitutes an eigenvalue problem which determines the value of c. It can be shown [20] that the unique wave speed is

$$c = \left[\frac{AD_1}{2}\right]^{1/2} (N_2 - 2N_1) \qquad (28)$$

and the shape of the wave front is given by

$$N(\zeta) = \frac{N_2}{1 + K \exp\left[\left[\frac{A}{2D_1}\right]^{1/2} N_2\zeta\right]} . \qquad (29)$$

Because of translational invariance of Eq. (26), K is an arbitrary constant. It can be chosen so that $\zeta = 0$ corresponds to $N = N_2/2$, in which case $K = 1$. We can think of the axisymmetric wavelike solutions of (19) as having a

wave speed $c(r)$, a function of r, and asymptotically reaching the value $c(r) \sim c$ for large r.

Upon application of a voltage greater than u_n, a lateral spread of the discharge is expected to occur. The dependence of the speed of the spread on the applied voltage u can be obtained from (28). At $u_n \leq u \leq 0$, the speed is given by

$$c = \left[\frac{v_i g}{2} \right] \left[-\frac{\hat{\alpha}\lambda_T \alpha}{2b} \right]^{1/2} \left[1 - 3 \left[1 - \frac{8u}{9u_n} \right]^{1/2} \right] , \qquad (30)$$

where $\hat{\alpha} = d \ln \alpha / d \ln E$. The speed tends to zero when the voltage u approaches the value u_n and it rises with voltage if the voltage is in excess of this value. The spread of the cathode spot edge occurs due to lateral diffusion of electrons. The spread mechanism differs therefore from that investigated experimentally for a normal discharge when a voltage is applied which is higher than the normal cathode fall voltage [21]. In normal conditions, the propagation of the spot edge results from radial ion drift [11]. This case is studied in the following section.

B. Subnormal discharge with strong distortion of the field

In this section we consider the subnormal discharge in the regime when the cathode sheath is formed $d < L$. Equation (38), which resembles Eq. (19) above, will be obtained using the following assumptions: (a) the radial term in Poisson's equation can be neglected and the sheath length depends parametrically on the radial position; (b) the shape of the axial distribution of the ion space charge does not change with time; and (c) the flux of ions from the plasma into the sheath can be neglected. The effect of the normal current density and the appearance of subnormal oscillations are analyzed using this equation.

1. Balance of ions

The radial motion of ions cannot be neglected for a subnormal regime when the cathode sheath and plasma region are formed. The potential fall is concentrated in the cathode sheath the length of which is d. The plasma region can be treated as field free. The equation for the radial balance of ions can be obtained by integrating Eq. (1) with respect to z within the sheath

$$\int_0^d \frac{\partial n_i}{\partial t} dz + \Gamma_{iz}(r,0) + \Gamma_{iz}(r,d) + \frac{1}{r} \frac{\partial}{\partial r} r \int_0^d \Gamma_{ir}(r,z) dz$$
$$= \int_0^d I \, dz . \qquad (31)$$

For $d > L$ integration should be performed up to the anode. Equation (31) differs from Eq. (14) as the field distortion is taken into account. The different terms of (31) are calculated below.

The ion influx from the anode is absent $\Gamma_{iz}(r,L) = 0$. We assume that the ion influx from the plasma is also negligible, i.e., for both cases $d > L$ and $d < L$,

$$\Gamma_{iz}(r,d) = 0 . \qquad (32)$$

This assumption is valid for subnormal and normal regimes and is violated for the abnormal regime where the ion influx from the plasma may constitute a considerable part of the total ion flux in the sheath [22]. We will not consider here the abnormal discharge mode for which a great part of ionization occurs in the plasma [22] and in which the discharge covers the whole area of the cathode [9].

To calculate the ion fluxes in (31) it is necessary to know the two-dimensional distribution of the electric field in the sheath. We will suppose the potential distribution is of the form

$$\phi(z,r) = zE_c \left[1 - \frac{z}{2d} \right] . \qquad (33)$$

It corresponds to the solution of the Poisson equation (3) when both the radial term in (3) and the axial dependence of the ion space charge are neglected. Such an approximation is suggested by the numerical modeling (see Fig. 6). Both the field on the cathode E_c and the sheath length $d = E_c / 4\pi e n_i$ in (33) depend on radial position. According to (33), the axial and radial components of the electric field are

$$E_z(z,r) = E_c \left[1 - \frac{z}{d} \right] ,$$
$$E_r(z,r) = 2\pi e z \frac{dn_i}{dr} \times \begin{cases} (L-z) & \text{at } L < d \\ (d-z) & \text{at } L > d \end{cases} \qquad (34)$$

and the field at the cathode is given by

$$E_c(r) = \begin{cases} \dfrac{U}{L} \dfrac{2d}{2d-L} & \text{at } L < d \\[2mm] \dfrac{2U}{d} & \text{at } L > d . \end{cases} \qquad (35)$$

Using Eq. (34), we find the integrated radial ion flux

$$\int_0^L \Gamma_{ir}(r,z) dz = \begin{cases} \dfrac{\pi e \mu_i L^3}{3} n_i \dfrac{dn_i}{dr} & \text{at } L < d \\[3mm] \dfrac{\pi e \mu_i d^3}{3} n_i \dfrac{dn_i}{dr} & \text{at } L > d . \end{cases} \qquad (36)$$

The ion flux at the cathode surface is found from Eq. (35)

$$\Gamma_{iz}(r,0) = \mu_i n_i E_c = \mu_i n_i \times \begin{cases} \dfrac{U}{L} \dfrac{2d}{2d-L} & \text{at } L < d \\[2mm] \dfrac{2U}{d} & \text{at } L > d . \end{cases} \qquad (37)$$

The right-hand side of (31) is proportional to the electron reproduction coefficient $\eta = \gamma(M-1)$; the multiplication M is calculated in the Appendix.

Using Eqs. (31), (32), (36), (37), and (A8) and introducing the dimensionless density $N = 2\pi e n L^2 / U$ and voltage $\tilde{U} = U/BpL$, we obtain the time-dependent diffusion equation

$$f(N) \frac{\partial N}{\partial t} - \frac{1}{r} \frac{\partial}{\partial r} r D(N) \frac{\partial N}{\partial r} = F(N, \tilde{U}) , \qquad (38)$$

with a source term

$$F(N,\widetilde{U})=\frac{\mu_i U}{L^2}N(\eta-1)\times\begin{cases}(1+N) & \text{for } N<1 \\ 2N^{1/2} & \text{for } N>1\end{cases}$$

and the nonlinear diffusion coefficient

$$D(N)=\frac{\mu_i U}{6}\times\begin{cases}N & \text{for } N<1 \\ N^{-1/2} & \text{for } N>1 \ .\end{cases}$$

The function

$$f(N)=\begin{cases}1 & \text{for } N<1 \\ N^{-1/2} & \text{for } N>1\end{cases}$$

describes a decrease of the ion drift time through the sheath with reduction of the sheath length for $d<L$. The multiplication M from (A8) can be expressed in the form

$$M(\widetilde{U},N)=\exp\frac{ApL}{2\widetilde{U}N}\times\begin{cases}\mathcal{J}_{\text{Arh}}[\widetilde{U}(1+N)]-\mathcal{J}_{\text{Arh}}[\widetilde{U}(1-N)] & \\ \quad\text{for } N>1 & \text{(39)} \\ \mathcal{J}_{\text{Arh}}(2\widetilde{U}\sqrt{N}) & \text{for } N<1 \ .\end{cases}$$

At $N=1$ the sheath length is equal to the gap length.

The left-hand side of Eq. (38) describes the radial transport of ions which is formally diffusive with a nonlinear diffusion coefficient $D(N)$. The source F on the right-hand side includes the production of ions by ionization and ion losses to the cathode surface. This term is proportional to the departure of the electron reproduction coefficient from unity; unity is the equilibrium value of η for a steady-state radially inhomogeneous discharge. At $pL>(pL)_{\min}$ the ionization coefficient α is a rapidly varying function of the field, while the multiplication M and reproduction coefficient η depend on α exponentially. Therefore, small changes in N or in $\widetilde{U}$ are already sufficient for η to be appreciably greater than unity and for the characteristic time for the density rise to be of the order of $\eta\tau_i$. Equation (38) resembles Eq. (19) with the exception of the functional dependence of the source term and the value of the diffusion coefficient.

2. Steady-state and traveling wave solutions

The methods developed above in Secs. IV A 3 and IV A 4 can be applied here.

Introducing a new function of density $\Phi=2\int_0^N D(N)dN$, the steady-state version of Eq. (38) for Φ can be reduced to Eq. (20) with the diffusion coefficient $D_0=\mu_i U/6$, the right-hand side being given by

$$F(\Phi,\widetilde{U})=\frac{\mu_i U}{L^2}(\eta-1)\times\begin{cases}2\Phi^{1/2}(1+\Phi^{1/2}) & \text{at } \Phi<1 \\ (\Phi+3)^3/16 & \text{at } \Phi>1\end{cases}\quad(40)$$

and with the multiplication M from Eq. (39). The analogy with the particle motion discussed in Sec. IV A 3 can therefore be used in this case. The force $F(\Phi,\widetilde{U})$ and its potential $V(\Phi,\widetilde{U})$ are shown in Fig. 10 for discharge conditions corresponding to the formation of a normal cathode spot.

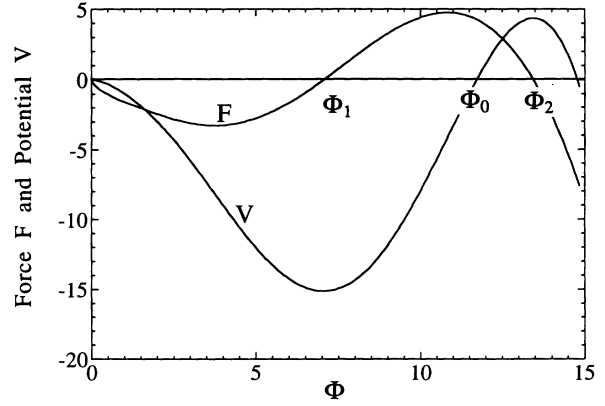Figure 11 shows the current dependence of the radial distributions of ion density for two values of pL. In the

FIG. 10. The force $F(\Phi,\widetilde{U})$ acting on the particle and its potential $V(\Phi,\widetilde{U})$, in arbitrary units. Discharge parameters correspond to normal conditions [curve 5 in Fig. 11(a)]. The particle starts in the vicinity of the potential maximum $\Phi=\Phi_0$, is accelerated in the region $\Phi_0<\Phi<\Phi_1$, and is slowed down in the region $0<\Phi<\Phi_1$. The effect of the cylindrical geometry leads to a positive value of $V(\Phi_0,\widetilde{U})$.

vicinity of the Paschen minimum $pL\sim(pL)_{\min}$, the radial distributions of the ion density remain almost unchanged while the current rises [Fig. 11(b)]. For higher pL, an increase of the current is accompanied by a lateral constriction of the discharge [Fig. 11(a)]. When the density in the center reaches the value corresponding to the maximum electron multiplication (see Fig. 15), a lateral expansion of the spot occurs [see curves 5 and 6 in Fig. 11(a)].

Calculated static current-voltage characteristics in the subnormal glow region are plotted in Fig. 12 for two pressures. They are obtained as steady-state solutions of the time-dependent Eq. (38) for different values of the resistance R_c. To model the hysteresis loop, the resistance was slightly changed and the previous solution was used as an initial condition for the next one. The voltage jumps that are observed for the generator voltage $U_s=265$ V are shown by dashed lines.

Experimental investigations of the lateral spread of the normal discharge have been summarized by Emeleus and von Engel [21]. The speed of the discharge edge increases with the degree of anomalousness, i.e., the amount of the voltage excess with respect to the normal cathode fall. The theory proposed by Hollo and Nuiry [11] uses an equation similar to Eq. (38) to describe the discharge spread at constant voltage. The approach developed in Sec. IV A 4 can be used as Eq. (38) resembles Eq. (19) and their right-hand sides exhibit similar behavior.

3. Subnormal oscillations

If the discharge maintaining voltage changes with time, new phenomena can be observed. A finite delay of the voltage feedback due to presence of displacement current and the capacitance of the external circuit may cause the appearance of current oscillations. The subnormal oscillations are studied in this section.

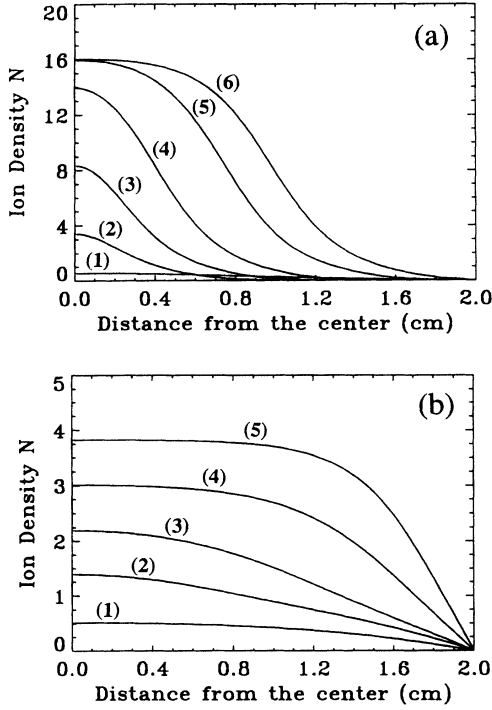The contribution of the displacement current to the to-

FIG. 11. Radial distributions of the dimensionless ion density N approached as steady-state solutions of Eq. (38) for different currents. (a) $p = 2.4$ Torr, currents and voltages: (1) 6.27 μA, 174.9 V; (2) 6.12 μA, 141.83 V; (3) 19.5 μA, 118.8 V; (4) 64.29 μA, 112.0 V; (5) 192 μA, 110.6 V; (6) 320 μA, 110.35 V. (b) $p = 0.9$ Torr, currents and voltages: (1) 11.9 μA, 174.9 V; (2) 37.7 μA, 112.9 V; (3) 71.5 μA, 112.4 V; (4) 178 μA, 115.5 V; (5) 352 μA, 112 V. The discharge voltages are given because of the hysteresis loop.

tal current J at the cathode surface is given by

$$2\pi e \int_0^R d\,dr \left[j + \frac{1}{4\pi e} \frac{\partial E_c}{\partial t} \right] = J \ , \tag{41}$$

where E_c is the field at the cathode and j is the conduction current density. The presence of a capacitance C_0 in the external circuit modifies Eq. (5)

$$C_0 \frac{\partial U}{\partial t} = \frac{U_s - U}{R_c} - J \ . \tag{42}$$

Equations (41) and (42) can be combined giving

$$\frac{\partial U}{\partial t} + \frac{J_c}{C} = \frac{U_s - U}{\tau} \ , \tag{43}$$

where distortion of the field is neglected and the time constant $\tau = R_c C = R_c(R^2/4L + C_0)$ is introduced. The conduction current is given by

$$J_c = (1+\gamma)2\pi e \mu_i \int_0^R n_0(r)E_c r\,dr \ . \tag{44}$$

Since usually $C_0 \gg R^2/4L$, Eq. (43) can be applied to the entire subnormal region [4].

The discharge behavior is characterized by two time scales. The time scale τ defines the delay of the voltage
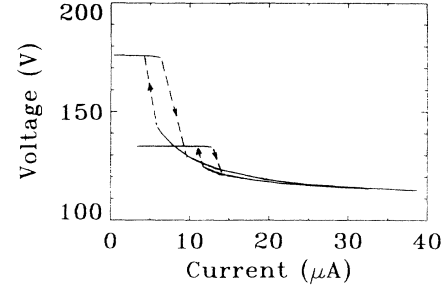

FIG. 12. Static current-voltage characteristics for $p = 2.4$ and $p = 0.9$ (Torr) with $\gamma = 0.1$. The dashed lines indicate the voltage jumps observed for the voltage of generator $U_s = 265$ V.

feedback. As a result of this delay, the departure of the electron reproduction η from unity (the equilibrium value) is not damped but increases with time. The rate of the density growth according to (38) is on the time scale $\sim \tau_i/(\eta-1)$. Owing to a strong dependence of $\eta(U)$ on U, a small increase of U is already sufficient for η to be appreciably greater than unity and for the density to increase rapidly on the time scale τ_i or even faster. Typical results from the numerical solution of the set of Eqs. (38) and (43) are shown in Figs. 13 and 14. Different shapes of current oscillations can be obtained for different discharge conditions: small amplitude oscillations (Fig. 13), relaxation oscillations, or a periodic breakdown (Fig. 14). The shape of the oscillations depends on the ratio
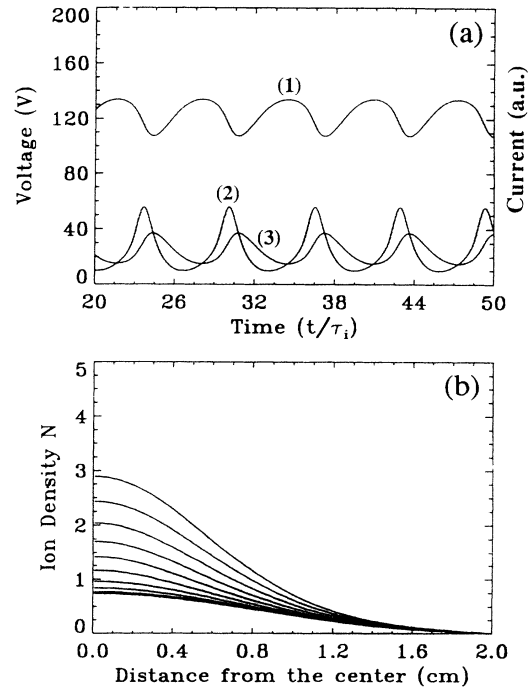

FIG. 13. (a) Subnormal oscillations of small amplitude for $\gamma = 0.1$, $R = 2$ cm, $pL = 1.3$ Torr cm, $U_s = 152$ V, $C = 10$ pF, and $\tau = 1.5\tau_i$. (a) 1, voltage; 2, conduction current; 3, total current. (b) Radial distributions of the dimensionless ion density for ten different times between a maximum and a minimum of the voltage.

FIG. 14. Relaxation subnormal oscillations for $\gamma = 0.1$, $R = 2$ cm, $pL = 1.8$ Torr cm, $U_s = 177$ V, $C = 10$ pF, and $\tau = 2\tau_i$. (a) 1, voltage; 2, conduction current; 3, total current. (b) Radial distributions of the dimensionless ion density for ten different times between a maximum and a minimum of the voltage.
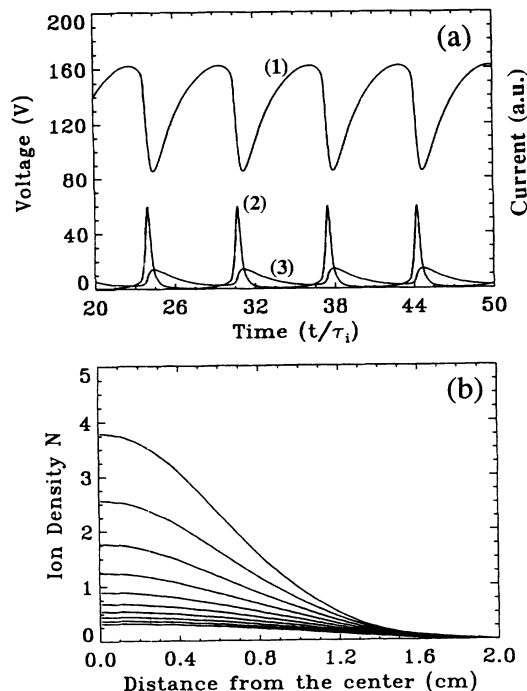
τ / τ_i as well as on the value of pL. The radial distributions of ion density for different phases of the oscillations are shown in Figs. 13(b) and 14(b). It is seen that the radial distribution changes significantly during the period, i.e., the current oscillations represent a two-dimensional phenomenon.

The boundaries of oscillation (dis)appearance are affected by the parameters of the external circuit. The region of oscillation is expanded with increase of the capacitance C_0 in accordance with the experimental observations [5]. For small values of C_0 the static current-voltage characteristics are obtained with a hysteresis loop (Fig. 12). As C_0 increases, the low-current boundary of the region of oscillation shifts toward lower currents. The increase of C_0 also degrades the stability of the normal discharge. This influence shows up with current decrease when the transverse dimensions of the normal cathode spot become so small that further reduction of current is accompanied by an increase in the voltage.

V. DISCUSSION OF RESULTS

The applicability of the fluid model for the description of slow electrons can be understood as follows. Generally, the fluid approximation is valid when the characteristic spatial scale exceeds the electron energy relaxation length. For atomic gases, in which the elastic collisions with gas atoms are the only mechanism for the energy relaxation of electrons with energies w below the excitation potential, the energy relaxation length is given by

$\lambda_\varepsilon = \lambda / \sqrt{\delta}$, where λ is the electron mean free path, $\delta = 2m/M \ll 1$ is the energy loss in elastic collisions, and m and M are the electron and ion masses. For argon at $p = 10$ Torr this length $\lambda_\varepsilon \sim 0.2$ cm is small compared to the gap length L, hence only the region of length λ_ε in the vicinity of the anode should be treated kinetically [23]. At $p = 3$ Torr the length $\lambda_\varepsilon \sim 0.7$ cm is of the order of the gap length. When λ_ε exceeds the plasma dimensions, the slow electrons move with conservation of their total energy (kinetic plus potential) [22]. This results in the appearance of standing striations in subnormal discharges [7,24] with the potential difference between striations being roughly equal to the excitation potential of the gas. It is desirable to emphasize that the potential contours for subnormal discharges have not been measured experimentally, but the observable striations make the optical mapping of equipotentials possible [24]. In the presence of the potential well (as in Fig. 7) which captures the slowest electrons, and in the absence of electron-electron collisions, the electrons are divided into two almost independent groups: trapped and free. As the densities of trapped and free electrons change in an entirely different manner, the mean energy (temperature) of slow electrons is spatially inhomogeneous [22]. To our knowledge, no spatially resolved measurements of the electron energy distribution function for these conditions have been carried out up to now.

The structure of the plasma region can be treated as follows. The plasma density profile can be described by the ambipolar diffusion equation with the density at the sheath edge equal to the ion density in the sheath and the density at the anode equal to zero. The nonlocality of the ionization which is to be taken into account for near-normal regimes results in the formation of a maximum in the plasma density at the end of the negative glow region (see Fig. 7). The condition of quasineutrality $n_e \approx n_i \approx n$ defines the distribution of the potential in the plasma. The potential can be divided into two parts: the ambipolar potential $\phi_a = -T_e \ln(n)$ and the "current" potential ψ, which satisfies the current conservation equation $\text{div}(n \, \text{grad}\psi) = 0$ and is responsible for the current. The sheath edge and the anode are equipotential lines for ψ. In this way, the appearance of the maximum and saddle points in the potential distribution obtained from numerical modeling (Fig. 7) can be understand qualitatively.

We turn now to discussion of the results obtained from the analytical model.

The question of whether diffusion of charged particles plays a decisive role in the formation of structures on the cathode of a glow discharge has been widely discussed (see [16] and references therein). Our results show that both radial diffusion of electrons and ion drift in the radial field may lead to the formation of the cathode spot. The former mechanism dominates at low currents, when the Poisson length exceeds the gap length. The latter manifests itself at enhanced currents when the field distortion is essential. Their magnitude is of the same order at $N = 6T_e/U \ll 1$ when the diffusion coefficients in Eqs. (19) and (38) are equal.

The equations obtained for the lateral distribution of the space charge in both these cases coincide formally

with the cylindrically symmetrical Fisher equation [20]. For a time-independent maintaining voltage, the steady-state and traveling wave solutions have been analyzed qualitatively using the analogy with particle motion under the influence of a force. The character of the possible solutions was shown to be essentially dependent on the topology of the nonlinear source term, which is influenced by discharge conditions.

The source term is proportional to the departure of the electron reproduction coefficient from its equilibrium value defined by the balance of electron multiplication, which is necessary to sustain the discharge. The dependence of the electron multiplication on the sheath length has been calculated using the local approximation for the Townsend ionization coefficient as well as using a simple model for nonlocal ionization. On the left branch of the Paschen curve, the multiplication increases monotonically with the rise in the sheath length. On the right branch, for a given voltage, the multiplication exhibits a maximum as a function of the sheath length when the field on the cathode goes through the value corresponding to saturation of the ionization coefficient and the sheath length becomes shorter than the range of the fast electrons. The results of the local and nonlocal approaches are found to be close to each other for the subnormal glow region and differ significantly for the region of abnormal discharges. The existence of the multiplication maximum is the reason for the existence of normal glow discharges: the normal cathode spot is formed in such a way that multiplication reaches the maximal value [16]. Hence the normal cathode spot can be formed only on the right branch of the Paschen curve where the multiplication exhibits a maximum.

A phenomenon that is analogous to the normal-current-density effect is predicted to exist in the subnormal glow region if the secondary emission coefficient is an increasing function of the electric field and if the operating point lies between the minimum of the Paschen curve and the point where $\alpha''(E)=0$. In this case also the multiplication can reach a maximum as a function of the ion space charge and a cathode spot can be formed. The difference between the phenomena of normal and subnormal spots is due to different kinds of lateral losses. The shape of the subnormal spot is governed by diffusion of electrons while the normal cathode spot is formed under the influence of the transport of ions in radial field. With an increase of the voltage in excess of the normal value, a lateral spread of the spot was found.

For a time-dependent maintaining voltage, new phenomena appear. Due to the presence of the displacement current and the capacitance of the external circuit, the voltage feedback is characterized by a finite delay and causes the appearance of subnormal oscillations. The subnormal oscillations are recognized as two-dimensional phenomena. The mechanism of their excitation and a sequence of events can be identified as follows. A local increase of the ion space charge results in an increase of the electron multiplication, which in the subnormal regime cannot be stabilized by the lateral losses of ions. A stable state can only be achieved when the ion density reaches the value corresponding to the maximum multiplication.

If the discharge sustaining voltage at this time exceeds the value corresponding to the normal cathode fall voltage, lateral spread of the discharge occurs. In fact, such a behavior appears in our calculations for large values of the capacitance C. For small values of C, an increase of the ion density is accompanied by a voltage decrease. The rate of the voltage feedback is characterized by the time τ. When this time is of the order of the rate of discharge development (which is of the order of τ_i) the ion density begins to decrease before reaching the maximal value corresponding to normal conditions. The oscillations occur therefore for two reasons: (a) the local instability of the sheath in the subnormal region and (b) the finite relaxation time of the discharge maintaining voltage. The shape of the oscillations is determined by these two time scales. For small τ, the oscillations are not excited in the whole transition region. In this case, a hysteresis loop in the current-voltage characteristics appears in the calculations (see Fig. 12). The experimental data [7] show more pronounced hysteresis behavior of the discharge due to gas heating, which was neglected in our model.

VI. SUMMARY

The subnormal region of direct current glow discharges in a cylindrical chamber between two parallel electrodes has been investigated by means of both two-dimensional numerical modeling and a simplified quasi-one-dimensional approach. The formation of the lateral structure of the discharge and the appearance of current oscillations were explained. The methods developed can be used for the investigation of more complex spatial patterns observed in the near-electrode regions of glow discharges. The results obtained should stimulate the experimental investigation of the subnormal glow region using modern methods.

ACKNOWLEDGMENTS

APPENDIX

The concept of Townsend ionization coefficient α, defined as an average number of ionizing collisions per unit distance of drift, may be used in the range of E/N, where the electrons attain an equilibrium drift velocity in the electric field. These conditions are not satisfied at high E/N reached for a Townsend discharge on the left branch of the Paschen curve [25,26] or in the fully developed cathode sheath [22]. Consequently, in these cases the energy of an electron is a function of the distance, therefore ionization depends on the spatial position. Hence it is necessary to calculate the electron multiplication M as a function of position in the gap. For a Townsend discharge M has been calculated in Ref. [25]

by means of Monte Carlo simulation of fast electrons assuming predominantly forward electron scattering. A simple method of calculating M for a spatially unhomogeneous electric field in the cathode region of glow discharges is given below.

The energy balance of fast electrons can be described using a continuous-energy-loss approximation [27]

$$\frac{dw}{d\xi} = eE(z,r) - NL(w) \, , \tag{A1}$$

where w is the electron kinetic energy, N the gas density, $L(w)$ the energy-loss function, and ξ the fast electron path along its trajectory. The loss function corresponds to a mean retarding force acting on the electron due to energy losses from excitation and ionization of the gas. In argon it has a weak maximum at energies of about three times the electron excitation threshold [28] and is

assumed to be energy independent below $L(w)=L_0=5\times10^{-14}$ eV cm^2. The electrons can be divided into two groups according to their origin. The first group represents electrons generated in the high-field region $eE>NL_0$. The second group consists of those appeared in the low field region where the retarding force is less than the accelerating force $eE<NL_0$. The electrons of the first group are runaway and produce nonlocal ionization in the low field region $eE<NL_0$. Ionization by these fast electrons is proportional to their flux [22]

$$I = \alpha_{\text{eff}}\Gamma_f \, , \tag{A2}$$

where $\alpha_{\text{eff}} = NL_0/\varepsilon_0$ is an effective Townsend coefficient and $\varepsilon_0 = 29$ eV the energy loss per ion-electron pair [28].

Neglecting both the scattering of fast electrons and the radial component of field, the flux of fast electrons can be obtained [22] in the form

$$\Gamma_f(z) = \tilde{\Gamma} \times \begin{vmatrix} \exp(\alpha z) & \text{at } 0<z<\tilde{d} \\ \exp[\alpha(2\tilde{d}-z)] & \text{at } \tilde{d}<z<d \\ \exp\left\{\alpha\tilde{d}\left[1-\left(1-4\Lambda\frac{\Lambda-z}{(2\Lambda-d)^2}\right)^{1/2}\right]\right\} & \text{at } d<z<\Lambda \, , \end{vmatrix} \tag{A3}$$

where d is the sheath length, $\tilde{d}=d(1-d/2\Lambda)$ is the boundary between high and low field regions, $\Lambda = U/NL_0$ is the fast electron range, and Γ is the electron flux at the cathode. The value of $NL_0 = 170$ V cm^{-1} coincides approximately with the field at the Paschen minimum $Bp = 180$ V cm^{-1} and the value $\alpha_{\text{eff}} = 6$ cm^{-1} is of the order of $\alpha(NL_0)=4.4$ cm^{-1}. On the left branch, $\Lambda > L$ and the electron runaway should be taken into account [25,26]. On the right branch, $\Lambda < L$ and nonequilibrium conditions exist after the field on the cathode exceeds the value of NL_0.

The slow electrons are those generated in the low field region where retarding force is less than the accelerating force $\tilde{d}<z<d$. They are roughly in equilibrium with the field. The ionization they produce is therefore determined by the local field, with ionization coefficient $\alpha(E)$ depending strongly on the field strength. Since the slow electron flux is equal to zero at $z<\tilde{d}$, the total electron flux Γ_e coincides with Γ_f at $z<\tilde{d}$. At $z>\tilde{d}$ it is given by

$$\frac{d\Gamma_e}{dz} = \alpha(E)(\Gamma_e-\Gamma_f) + \alpha_{\text{eff}}\Gamma_f \, . \tag{A4}$$

Integrating (A4), we find the total electron flux at $z>\tilde{d}$

$$\Gamma_e = \Gamma\exp\left[\alpha\tilde{d} + \int_{\tilde{d}}^z\alpha(E)dz\right]$$
$$+ \int_{\tilde{d}}^z[\alpha_{\text{eff}}-\alpha(E)]\exp\left[\int_{z'}^z\alpha(E)\right]\Gamma_f dz' \, . \tag{A5}$$

The second term in (A5) describes the ionization by the fast electrons in the low field region. At $\Lambda>d$ the fast electrons produce nonlocal ionization in the plasma and at $\Lambda<d$ they contribute to the local ionization within the

sheath in the region $\tilde{d}<z<2\tilde{d}$.

On the left branch of the Paschen curve $L<\Lambda$, a portion of the fast electrons can reach the anode. Their losses on the anode result in a decrease of multiplication with reduction of pL

$$M = \exp(\alpha_{\text{eff}}L) \, . \tag{A6}$$

The maximal value of M is reached at $E\approx$ const, i.e., for a Townsend discharge. The distortion of the field leads to a decrease of M.

On the right branch the situation is opposite. The distortion of the field results in an increase of M. Using (A5) and noting that $\alpha(E)$ is a rapidly varying function of E, we obtain, for $2\tilde{d}<d$,

$$M = \exp\left[\alpha\tilde{d} + \int_{\tilde{d}}^d\alpha(E)dz'\right] + \frac{\alpha_{\text{eff}}}{\Gamma}\int_{\tilde{d}}^{2\tilde{d}}\Gamma_f dz' \, . \tag{A7}$$

The second term in (A7) is due to fast electron contribution to ionization in the low field part of the sheath. For $\Lambda>d$ nonlocal ionization is partly produced in the plasma and the upper limit of the integral should be changed to Λ. The multiplication calculated according to (A7) exhibits a maximum as a function of sheath length (Fig. 15, curve 1).

Using the local approximation for Townsend's coefficient $\alpha(E)= Ap\exp(-Bp/E)$, we obtain the multiplication [11]

$$M_1 = \exp\frac{ABp^2}{4\pi en}\left[\mathcal{J}_{\text{Arh}}\left(\frac{E_c}{Bp}\right) - \mathcal{J}_{\text{Arh}}\left(\frac{E_a}{Bp}\right)\right] \, , \tag{A8}$$

where $E_a = (U/L)[(d-L)/(2d-L)]$ is the field at the anode at $L<d$ or zero at $L>d$ and $\mathcal{J}_{\text{Arh}}(x)$ is the "Ar-
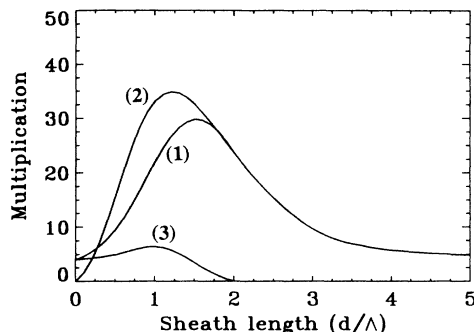
FIG. 15. Electron multiplication $(M-1)$ as a function of the reduced sheath length (d/Λ) for $L=3\Lambda$: (1) according to Eq. (A7) with the contribution of nonlocal ionization, $L_0 = 5\times10^{-14}$ eV cm^2, $\varepsilon_0 = 29$ eV; (2) according to Eq. (A8) with the local approximation for Townsend ionization coefficient, $Ap = 12$ cm^{-1}, $Bp = 180$ V cm^{-1}; (3) the contribution of nonlocal part [see Eq. (A7)].

rhenius integral"

$$\mathcal{J}_{\mathrm{Arh}}(x) = \int_0^x \exp\left[-\frac{1}{y}\right] dy \ .$$

The multiplication calculated using (A8) is shown in Fig. 15 (curve 2) for comparison. The region $\Lambda < 2d$ corresponds to local ionization. In the limit $d \gg L$, the multiplication is given by (A6) with substitution $\alpha(E)$ in place of α_{eff}.

Both curves 1 and 2 in Fig. 15 have maxima as a function of reduced sheath length at d/Λ about unity. The difference between results of local and nonlocal approaches is essential in the region corresponding to abnormal discharges $d < \Lambda$. In the limit of a strongly abnormal regime $d \ll \Lambda$, essentially all ionization is produced in the plasma region. Equation (A7) gives $M = U/\varepsilon_0$ while the local approach (A8) gives $M_1 = 0$. In the region of subnormal discharges $\Lambda < d$, the difference between (A7) and (A8) is not very important, so relationship (A8) has been used for convenience.

[1] B. N. Klyarfeld, L. G. Guseva, and A. S. Pokrovskaya-Soboleva, Zh. Tekh. Fiz. **36**, 704 (1966) [Sov. Phys. Tech. Phys. **11**, 520 (1966)].

[2] K. G. Emeleus, Z. Phys. **268**, 175 (1974); V. V. Vlasov, L. G. Guseva, and B. N. Klyarfel'd, in *Contributed Papers of the Tenth International Conference on Ionization Phenomena in Gases*, edited by D. Parsons (Oxford University Press, London, 1971), p. 98.

[3] L. A. Sena and O. L. Ryazantzeva, Zh. Tekh. Fiz. **48**, 1643 (1978) [Sov. Phys. Tech. Phys. **23**, 930 (1978)].

[4] V. N. Melekhin and N. Yu. Naumov, Zh. Tekh. Fiz. **54**, 1521 (1984) [Sov. Phys. Tech. Phys. **29**, 888 (1984)].

[5] V. N. Melekhin, N. Yu. Naumov, and N. P. Tkachenko, Zh. Tekh. Fiz. **57**, 454 (1987) [Sov. Phys. Tech. Phys. **32**, 274 (1987)].

[6] Z. Lj. Petrovic and A. V. Phelps, Phys. Rev. E **47**, 2806 (1993); B. M. Jelenkovic, K. Rozsa, and A. V. Phelps, *ibid.* **47**, 2812 (1993); A. V. Phelps, Z. Lj. Petrovic, and B. M. Jelenkovic, *ibid.* **47**, 2825 (1993).

[7] I. D. Kaganovich, M. A. Fodotov, and L. D. Tsendin, Zh. Tekh. Fiz. **64**, 22 (1994) [Tech. Phys. **39**, 241 (1994)].

[8] V. A. Schweigert, Pis'ma Zh. Tekh. Fiz. **19**, 56 (1993) [Tech. Phys. Lett. **19**, 659 (1993)]; Zh. Tekh. Fiz. **63**, 29 (1993) [Tech. Phys. **38**, 384 (1993)].

[9] A. Fiala, L. C. Pitchford, and J. P. Boeuf, Phys. Rev. E **49**, 5607 (1994).

[10] Yu. P. Raizer, *Gas Discharge Physics* (Springer-Verlag, Berlin, 1991).

[11] S. Hollo and B. Nyiri, Acta Phys. Hung. **72**, 71 (1992).

[12] E. A. Den Hartog, D. A. Doughty, and J. E. Lawler, Phys. Rev. A **38**, 2471 (1988).

[13] M. Surendra, D. B. Graves, and L. C. Plano, J. Appl. Phys. **71**, 5189 (1992).

[14] G. J. Parker, W. N. G. Hitchon, and J. E. Lawler, Phys. Lett. A **174**, 308 (1993).

[15] J. P. Boeuf, J. Appl. Phys. **63**, 1342 (1988).

[16] Yu. P. Raizer and S. T. Surzhikov, Teplofiz. Vys. Temp. **26**, 428 (1988) [High Temp. (USSR) **26**, 304 (1988)].

[17] M. Benilov, Phys. Rev. A **45**, 5901 (1992).

[18] K. G. Muller and G. Tenschert, Z. Phys. **178**, 319 (1964).

[19] K. G. Muller, Phys. Rev. A **37**, 4836 (1988).

[20] J. D. Murray, *Mathematical Biology*, Biomathematics Vol. 19 (Springer, Berlin, 1989).

[21] K. G. Emeleus and A. von Engel, J. Phys. D **12**, 555 (1979).

[22] V. I. Kolobov and L. D. Tsendin, Phys. Rev. A **46**, 7837 (1992).

[23] J. J. Lowke, J. H. Parker, and C. A. Hall, Phys. Rev. A **15**, 1237 (1977); L. D. Tsendin, Zh. Tekh. Fiz. **56**, 278 (1986) [Sov. Phys. Tech. Phys. **31**, 169 (1986)]; Yu. B. Golubovskii, V. I. Kolobov, and Sh. Kh. al Havat, *ibid.* **60**, 179 (1990) [*ibid.* **35**, 747 (1990)].

[24] K. G. Emeleus, Int. J. Electron. **39**, 177 (1975).

[25] J. D. Pace and A. B. Parker, J. Phys. D **6**, 1525 (1973); A. B. Parker and P. C. Johnson, Proc. R. Soc. London A Ser. **325**, 511 (1971).

[26] A. I. Pavlovskii, L. P. Babich, T. V. Loiko, and L. V. Tarasova, Dokl. Akad. Nauk SSSR **281**, 1359 (1985) [Sov. Phys. Dokl **30**, 303 (1985)]; L. P. Babich, T. V. Loiko, and V. A. Tsukerman, Usp. Fiz. Nauk **160**, 49 (1990) [Sov. Phys. Usp. **33**, 521 (1990)].

[27] K. G. Muller, Z. Phys. **169**, 432 (1962).

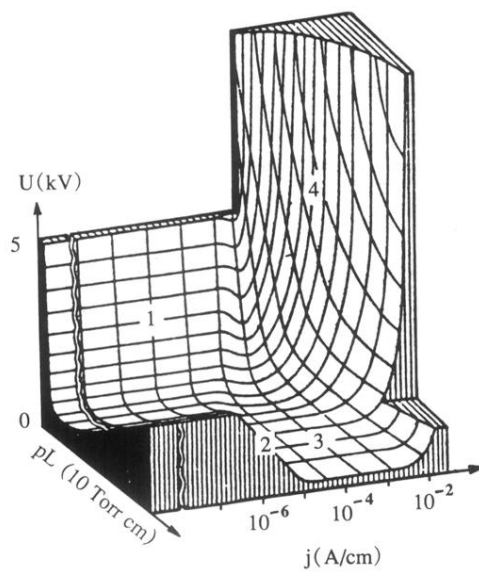[28] L. R. Peterson and J. E. Allen, J. Chem. Phys. **56**, 6068 (1972).

FIG. 1. Diagrammatic representation of different types of
glow discharges between plane-parallel electrodes (from Klyar-
feld, Guseva, and Pokrovskaya-Soboleva [1]). 1, Townsend
discharge; 2, subnormal discharge; 3, normal discharge; 4, ab-
normal discharge.